International Journal of Bioelectromagnetism
IJBEM
Volume 3, Number 2, pp. 39-48, 2001.

Accurate Reconstruction of Vessels from MR Images

Juan R. Cebral[(a)], Rainald Löhner[(a)], Peter J.Yim[(b)]

[(a)]*School of Computational Sciences, George Mason University, Fairfax,Virginia, USA*
[(b)]*Diagnostic Radiology Department,National Institutes of Health, Bethesda, Maryland, USA*

Correspondence: JR Cebral, School of Computatinoal Sciences, George Mason University,
4400 University Drive, MS 4C7, Fairfax, VA 22030 USA. E-mail: jcebral@gmu.edu, phone 703-993-4078, fax 703-993-4064

Abstract. Finite element calculations of arterial hemodynamics are valuable for understanding vascular diseases, enhancing diagnosis and surgical planning. Accurate reconstruction of vessel anatomies is critical for computational fluid dynamics modeling of blood flows. A methodology for constructing finite element grids from three-dimensional medical images is presented. The anatomical images are segmented using either a region growing approach or deformable models. Watertight models of bifurcating arteries are constructed by merging branches reconstructed independently, using an adaptive voxelization scheme. The surface model is then cut, smoothed, and optimized. Finite element grids of tetrahedral elements are generated directly from surface triangulations using an advancing front method. Adaptive background grids are used to specify an element size distribution that depends on the local curvature of the surface model. The methodology is illustrated with several examples including normal and diseased carotid arteries, renal arteries, and the circle of Willis.

Keywords: Hemodynamics; Grid Generation; Magnetic Resonance Angiography; Carotid Artery; Circle of Willis

1. Introduction

Arterial flow quantification and visualization are valuable for determining relationships between hemodynamic factors and progression of vascular disease [Zarins et al., 1983; Ku et al., 1985; Berger, 1993], enhancing image-based diagnosis [Milner et al., 1998; Steinman et al. 2000; Yim et al., 2000], planning surgical and interventional procedures [Taylor et al., 1999; Cebral et al., 2001], and training. Arterial models based on idealized geometries may fail to capture important flow features due to the strong dependence of the flow characteristics on the vessel geometry [Moore et al., 1999]. On the other hand, realistic patient-specific models can provide new insights into the arterial hemodynamics [Perktold et al., 1998; Quarteroni et al., 1998; Zhao et al., 2000], and are required for the purposes of diagnosis and surgical planning due to the large anatomical and physiologic variability among individuals [Taylor et al., 1998; Cebral et al. 2000]. Accurate reconstruction of the vessel lumen is critical for computational fluid dynamics (CFD) modeling of blood flow.

Vessel reconstruction from medical images is a challenging problem due to image artifacts, noise and limited resolution. A variety of vessel surface reconstruction algorithms have been devised. The simplest method is *iso-surface* reconstruction, in which all the vertices on the surface share the same interpolated intensity value [Cline et al., 1991]. However, the iso-intensity value has to be chosen by trial-and-error and a single value may not be valid for the entire vessel or vascular tree.

The *fuzzy connectivity* approach extends the conventional region-growing method [Cebral and Löhner, 1999; Cebral and Löhner, 2001] by assigning fuzzy membership to all points in the image rather than the binary Inside-Outside classification of conventional region growing. Tissue classes are identified by placing seed points at various points inside and outside of the vessels. The method has been found to be useful in the visualization of MRA using intra-vascular contrast where artery-vein overlap is considerable [Lei et al., 1999].

The *marker controlled watershed segmentation method* has been applied to a high-resolution CT image of the pulmonary arteries and a contrast-enhanced MRA of the thoracic aorta [Yim et al., 1998; Yim and Summers, 1999]. Boundaries of the marker-controlled watershed fall along the ridges in the intensity surface of the gradient magnitude image. The precise location of the watershed boundary is largely independent of the placement of the markers that indicate the interior and exterior of the vessel. Furthermore, smooth surfaces can be reconstructed from the watershed segmentation without resort to surface smoothing operations. However, image intensity within the carotid artery in Gd contrast-enhanced MRA may be highly inhomogeneous due to wide variation in flow rate. Due to this problem, the watershed segmentation is prone to large errors in vessels such as the carotid artery.

An invasive approach that combines biplane angiography and endovascular ultrasound data has recently been used to accurately reconstruct coronary vessels [Ilegbusi et al., 1999; Wentzel et al., 2000]. The ultrasound images provide cross-sectional information while the angiographic data is used reconstruct the vessel axis. Although this technique is able to reconstruct very accurately the lumen of a given artery, it cannot deal properly with bifurcations and severe stenoses [Wentzel et al., 2001].

Another methodology [Taylor et al., 2001] that has been successfully applied to the reconstruction of the abdominal aorta starts by probing the volumetric data with 2D slices normal to the vessel axis. Segmentation of the vessel lumen for each of these slices is the performed using thresholding or level set methods. The result is a set of contours along each arterial branch that are interpolated using analytic curves and stacked into analytical surface patches. The final model is the obtained by joining all the branches using solid modeling procedures. These methods tend to localize the largest errors at the arterial bifurcations where sharp intersections between branches can be obtained.

Promising results have been obtained from *deformable models* [Aylward et al., 1996; Frangi et al., 1999]. The surface reconstruction begins by determination of the axis of the vessels by ridge tracking. The surface is found by determining the radii associated with each point along the vessel axis using estimates of scale. Radius-based surfaces can be used as initializations for a mechanical-analog deformable model. This method, however, is highly dependent on the initialization of the vessel radii that may prove to be a problem with further testing.

Recently, a new approach that combines a semi-automated deformable model for vessel surface reconstruction and a method for joining surface triangulations, which is necessary at vessel bifurcations, has been presented [Yim et al., 2001]. While this method is not completely automatic, it avoids the problem of vessel overlapping encountered in the region-growing schemes. The merging of surface triangulations is made using an iso-surfacing technique combined with adaptive background grids [Cebral et al., 2001].

In the remainder of this paper we describe the application of region growing and deformable model segmentation for constructing realistic arterial models from MRA images that are used to generate finite element grids for CFD calculations of hemodynamics.

2. Material and Methods

Given their high degree of flexibility and automation, we have adopted unstructured grids based on tetrahedral elements for our CFD calculations. The process of constructing a finite element grid from medical images can be subdivided into the following stages: model reconstruction (image processing), solid modeling (surface processing), and grid generation. In what follows we review each of these steps.

2.1. Region Growing Segmentation

The *region growing* scheme marks all the voxels topologically connected to a given seed voxel interactively selected inside the desired vessel, and with intensity in the same range as the seed. The successful application of this approach depends on the specification of an appropriate seed and intensity range. The specification of these parameters must be done on a trial-end-error basis for each case. However, we have found useful to select the seed in the region with lowest intensity within the artery, and to use the intensity level of the seed as the lower bound of the intensity range. If no upper bound is specified, then all the voxels connected to the seed with intensities greater than that of the seed are marked. The main drawback of this approach is that it can produce 'leaks' or false intersections between vessels or other bright anatomical structures that are close in space. Combining the region growing operator with image-crop and contrast-enhancement (sharpening) operators can help in reducing this problem. The *image-crop* operation restricts all other image processing operations to a user-defined region of interest, i.e. a bounding box in 3D. The *sharpening* operator enhances the image contrast and reduces the noise present in the image.

Once the voxels in the interior of the desired vessels have been marked, a surface triangulation is created using either an *iso-surface* extraction algorithm (marching tetrahedra) or by *direct tessellation* of the boundary surface. For further details see [Cebral and Löhner, 2001].

2.2. Segmentation with Tubular Deformable Models

The *tubular deformable model* procedure [Yim et al., 2001] is based on a surface mesh that deforms towards points of high image-gradient intensity while maintaining smoothness of the surface. It is based on a coordinate system that is tubular in nature and that allows for curvature of the cylindrical axis. In contrast to previous models [Frangi et al., 1999], the vertices deform only in the radial direction and their position is described only by their radial location. This formulation of the deformation process eliminates bias towards forming tubes of smaller or larger diameter.

The deformation process is straightforward. First the location of each vertex is initialized to be the point along its radial path where the maximum of the gradient magnitude occurs. The gradient image is obtained by convolution of the image with the gradient of the normalized spherical Gaussian function. The radial function then deforms so as to minimize discontinuities in the vertex radial position along the surface while maximizing the proximity of the vertices to edges in the image. The deformations are applied simultaneously to all vertices and repeated until an equilibrium condition is obtained.

The cylindrical deformation process could be applied directly to the modified cylindrical coordinate system. However, bunching of vertices will occur where radial lines merge. Where such bunching occurs, the effective elasticity of the surface becomes significantly greater which reduces the surface smoothness. This effect is removed by merging vertices in the deformation process to match the merging of the radial lines. This precludes two vertices from co-existing on the same radial line.

In practice, the axis of the tubular deformable model is defined from a sequence of points along the center of the vessel identified by the user. Alternatively, a *skeletonization* schemes can be used to automate the process of vessel axis definition [Yim et al., 2000; Choyke et al., 2001]. For bifurcations, the surface is reconstructed by two applications of the procedure: one for the parent vessel and its continuation onto one branch and the second for the parent vessel and its continuation onto the second branch. We have found this method to be highly reliable in qualitative and quantitative studies.

2.3. Solid Modeling

The generation of finite element grids requires a watertight definition of the computational domain, i.e. a surface model with no holes, gaps, self-intersections or overlapping

components. Traditionally, analytical surface patches such as Coons or NURBS have been fitted to the reconstructed triangulation. Boolean operations between different components, e.g. to merge different arterial branches, can then be performed using available geometric modeling packages. Alternatively, we generate finite element grids directly from the surface triangulations. This implies further processing of the reconstructed models.

Boolean operations between surface triangulations are carried out using a volumetric technique [Cebral et al., 2001]. The basis of the method is the extraction of the zero-level iso-surface of a (signed) distance map defined on an adaptive background grid that covers the entire computational domain. The distance map is computed as the shortest distance from a background grid point to the domain surface. This methodology has been applied to *merge* carotid artery branches reconstructed independently using the tubular deformable model.

Small-scale imperfections in the reconstructed triangulation are then filtered using a non-shrinking *surface smoothing* algorithm [Taubin, 1995]. The basis of this scheme is the iterative application of a Laplacian operator, which is equivalent to the calculating the mechanical equilibrium of spring system between neighboring surface nodes. A modified version of this algorithm that considers forces between not only nearest neighbors of a given point but also other close points has been used to avoid self-intersections in vessels of small diameters [Cebral et al., 2000].

Several *surface cutting* operations can be used to cut arterial branches at selected locations. These cuts are performed in order to restrict the CFD analysis to a desired portion of the vessel tree. A method for cutting vessel branches along contours of geodesic distances to a given source point yields good results in regions far from bifurcations [Cebral et al., 2000]. These cuts tend to be normal to the vessel axis and can be restricted to one branch at a time (topological constraint). The point where the cut is performed can be specified interactively with only one mouse click. When this method fails to provide the desired results, planar cuts restricted by a bounding box are used. The cutting plane and the bounding box are both graphically defined by the user.

Before proceeding to the finite element grid generation, the quality of the surface triangulation is improved using a *mesh optimization* algorithm. Duplicated points, i.e. points that are very close in space, and degenerated elements, i.e. elements with a repeated node, are first identified and deleted. Large aspect ratio or very small elements are then removed from the triangulation using an edge-collapsing algorithm. Diagonal swaps are then performed between adjacent triangles in order to minimize the maximum angle of the triangular elements. These operations are prevented if the new configuration has a significantly different surface normal than the original configuration. For further details see [Cebral and Löhner, 2001].

2.4. Grid Generation

As mentioned above, we have developed algorithms to generate tetrahedral finite element grids directly from the reconstructed models [Löhner, 1996]. These procedures do not need an analytical surface representation of the computational domain. Rather, they operate directly on the *discrete data*, i.e. surface triangulation. We have found that this approach yields accurate surface grids and can be fully automated.

Given a desired element size distribution, the generation of a volumetric grid composed of tetrahedral elements begins by first creating a new triangulation of the domain surface. We have developed an advancing front method [Löhner, 1996; Löhner, 1997; Owen, 1998] that creates a surface mesh using the reconstructed model as a support surface. A *feature detection* algorithm is used to identify and preserve surface features such as ridges (i.e. edges shared by triangles with large deviation of their unit normals), and corner points (i.e. points connected to one or more than two ridges). *Linear or quadratic interpolation* is used to place the newly created points on the support surface. *Topological constraints* are used during the interpolation in order to avoid jumps between locally unconnected surface elements, e.g. between arterial branches that are very close in space.

The specification of the element size distribution is typically done using background grid and sources. In many cases, such as carotid arteries of normal subjects, using a uniform element distribution is usually acceptable. In these cases, the element size is selected in order to have a minimum number of elements across the smallest cross section of the model. However, in cases with geometric features of different scales, such as arteries with high degree of stenosis or larger vessel trees, this approach may result in a very large number of elements and therefore extremely long computing times. For this reason we have developed methods to specify element sizes based on the local curvature of the surface model, using *adaptive background grids* [Löhner and Baum, 1992]. The basic idea of the methodology is to refine the background grid close to the model surface and specify element sizes at the nodes of this mesh based from the local curvature of the closest surface. This approach tends to yield grids that contain roughly the same number of elements across any cross-section of the model.

3. Results

In this section we present several examples that illustrate the process of generating finite element grids for computational fluid dynamics calculations of hemodynamics from medical images.

3.1. Carotid Arteries

The methodology was first applied to the construction of realistic models of the carotid bifurcation of human subjects from Gd contrast-enhanced MRA images. The first of these cases corresponds to a normal subject. Fig. 1a shows the maximum intensity projection (MIP) of the anatomical images. The reconstructed model of the right carotid artery is shown in Fig. 1b. Deformable models were used to reconstruct the internal carotid artery (ICA) and the external carotid artery (ECA) independently. These branches were then merged using the adaptive voxelization method in order to create a watertight model of the carotid bifurcation. A detail of the reconstructed models of the ICA and ECA extending into the common carotid artery (CCA) are shown in Fig. 1c. The merged model of the bifurcation is shown in Fig. 1d. This model was then used as a support surface to generate a finite element grid of tetrahedral elements with a uniform element size distribution. The surface of the finite element mesh is shown in Fig. 1e.

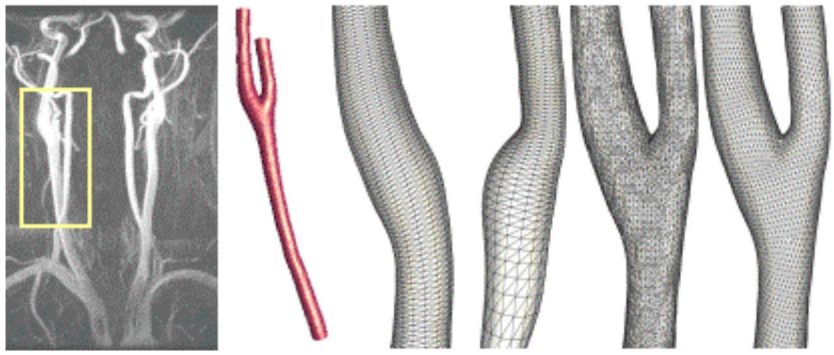

a) c) d) e)

Figure 1. Realistic carotid bifurcation model from MRA images of a normal subject: a) MIP projection of the MRA images; b) reconstructed model of the right carotid artery; c) model of the ICA and ECA extending into the CCA; d) bifurcation model after merging; e) surface of the final finite element grid.

The second case corresponds to the reconstruction of the carotid bifurcation from contrast-enhanced MRA images of a patient with atherosclerosis. As in the previous case, deformable models were used to reconstruct each arterial branch independently in order to avoid intersections with other close vessels present in the images. These branches were then merged into a watertight model and used as a support surface to generate a finite element grid with a uniform element size distribution. The MIP of the anatomical images is shown in Fig. 2a, the reconstructed model of the right carotid artery is shown in Fig. 2b and the surface of the final finite element grid is shown in Fig. 2c.

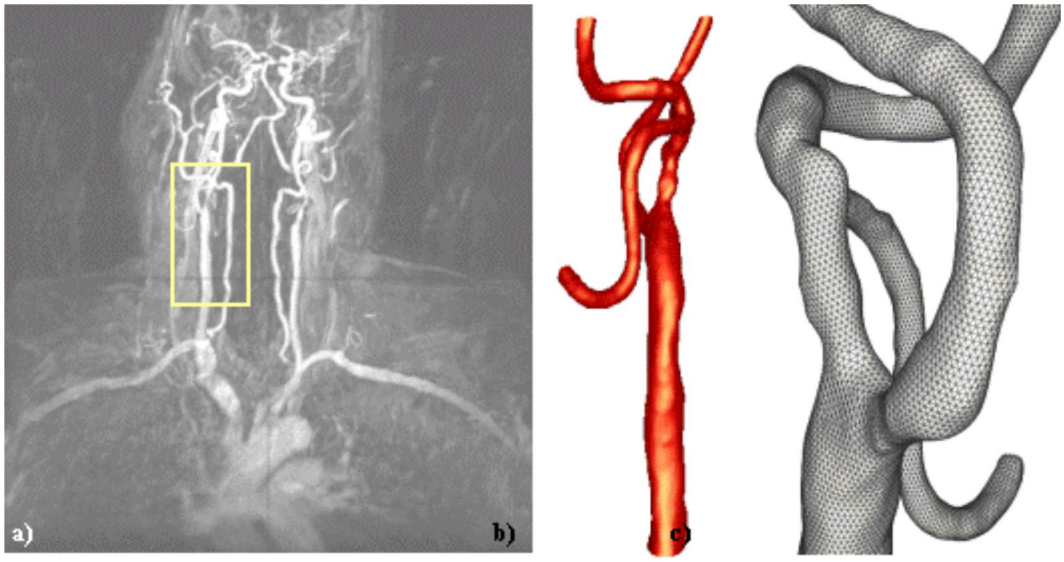

Figure 2. Construction of realistic carotid bifurcation model from MRA images of a patient with atherosclerosis: a) MIP projection of the contrast-enhanced MRA images; b) reconstructed model of the right carotid artery; c) surface of the final finite element grid.

A detail of the reconstructed models of the ICA and ECA extending into the CCA are shown in Fig. 3a and 3b, respectively. The surface triangulation of the bifurcation model after merging the ICA and ECA models is shown in Fig. 3c.

3.2. Renal Arteries

Tubular deformable models were used to reconstruct a portion of the abdominal aorta in the region of the renal arteries from contrast-enhanced MRA images (Fig. 4a). A deformable model was used for each branch and later all the branches were merged using the adaptive voxelization method. The watertight model thus created (Fig. 4b) was then used to generate a finite element grid with a uniform element size distribution (Fig. 4c).

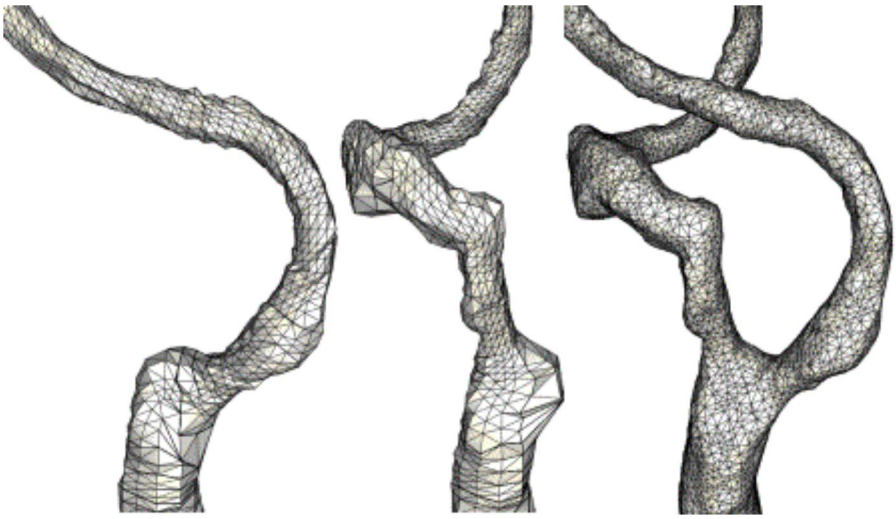

a) b) c)

Figure 3. Merging models of the ICA and ECA extending into the CCA in order to create a watertight model of the carotid bifurcation: a) model of the ICA; b) model of the ECA; c) merged bifurcation model.

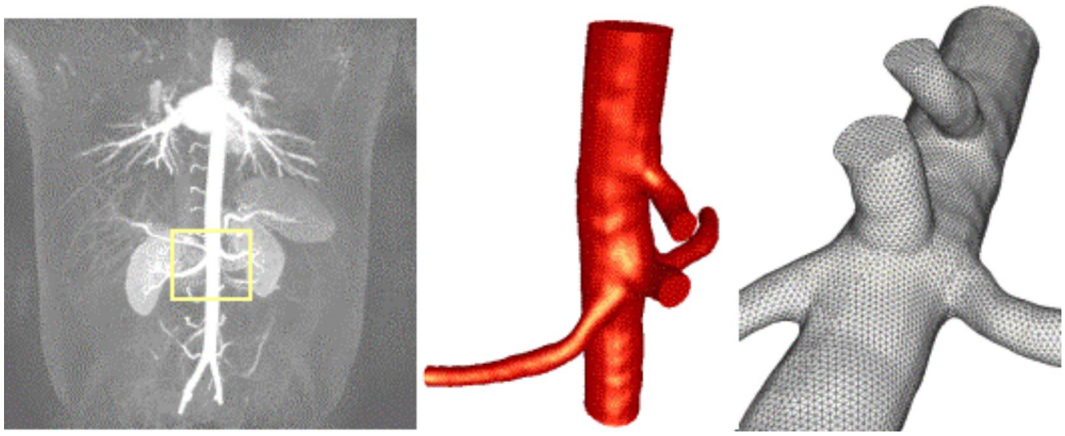

a) b) c)

Figure 4. Generation of a finite element grid of the renal arteries from contrast-enhanced MRA images: a) MIP of the anatomical images; b) reconstructed model; c) finite element mesh.

3.3. Circle of Willis

The region growing segmentation approach was applied to the construction of realistic anatomical models of the circle of Willis from 3D MRA images. The MIPs of the anatomical images before and after applying the region growing procedure are shown in Fig. 5a and 5b, respectively. The reconstructed model after smoothing and optimization is shown in Fig. 5c.

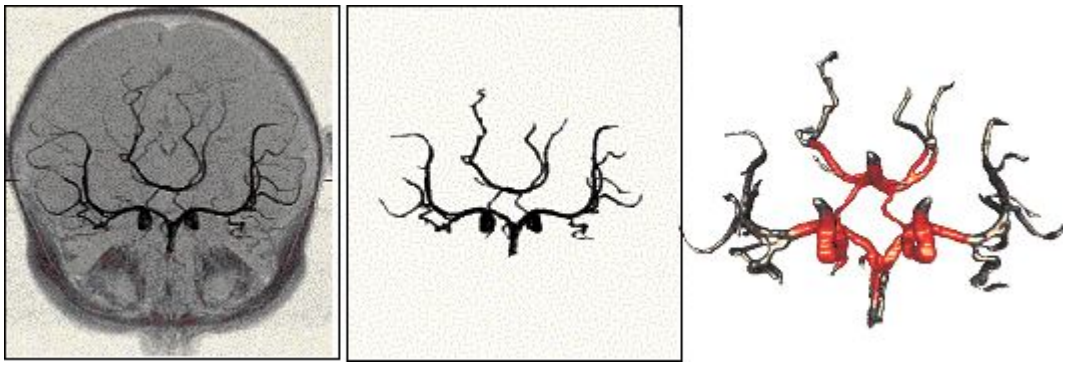

a) b) c)

Figure 5. Reconstruction of the circle of Willis from MRA images: a) MIP of original images; b) MIP after region growing; c) reconstructed surface model.

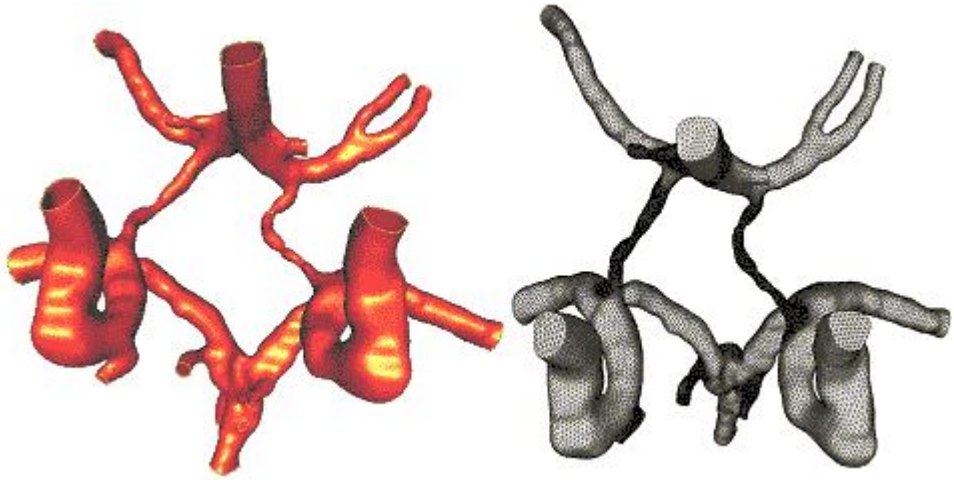

a) b)

Figure 6. Finite element grid of the circle of Willis: a) final geometrical model after cutting arterial branches; b) surface of the final finite element grid with uniform element size distribution.

The final geometrical model after cutting several arterial branches along contours of geodesic distances is shown in Fig. 6a. This model was then used to generate a finite element grid with uniform element size distribution. The final mesh (Fig. 6b) contained approximately 4 million elements.

A second case illustrates the use of adaptive background grids to specify an element size distribution that depends on the local surface curvature. Fig. 7a and 7b show the MIP of the MRA images from two different viewpoints. The reconstructed model is shown from similar viewpoints in Fig. 7c and 7d.

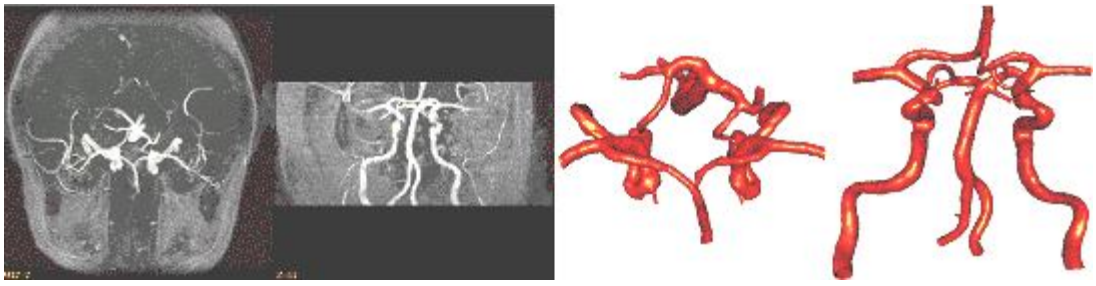

a) b) c) d)

Figure 7. Circle of Willis model reconstructed from MRA images: a) and b) MIP projections from different viewpoints; c) and d) reconstructed model from similar viewpoints.

A close-up view of the triangulation of the final model is shown in Fig. 8a. This triangulation was then used to refine an adaptive background grid based on its local curvature in order to specify an element size distribution that yields roughly the same number of elements across any cross-section of the model. The generated finite element grid (Fig. 8b) contained approximately 1 million elements.

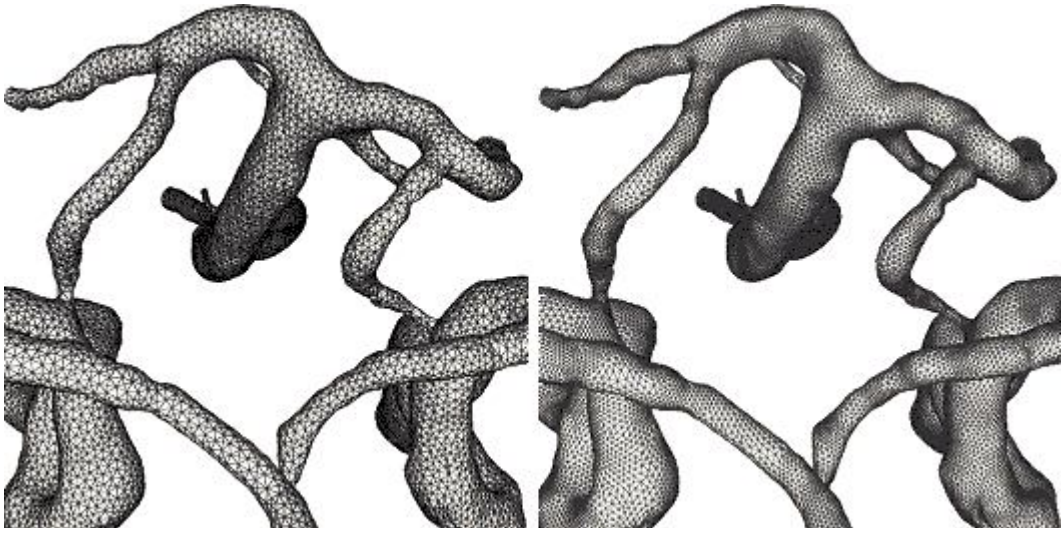

a) b)

Figure 8. Finite element mesh of the circle of Willis: a) surface triangulation of the final geometrical model; b) surface of the finite element grid generated using adaptive background grids to specify an element size distribution that depends on the local surface curvature.

4. Discussion

A methodology for generating finite element grids from medical images has been presented. The images are first segmented using either a region growing approach followed by an iso-surface extraction or using tubular deformable models. In the case of deformable models, each arterial branch is reconstructed independently, avoiding problems of intersections with other close anatomical structures, and then merged into a watertight surface using an adaptive voxelization scheme. The reconstructed triangulation is then cut at desired

locations, smoothed and optimized in order to improve the element quality. This final model is the used as a support surface for unstructured grid generation. A feature detection algorithm is combined with an advancing front method to generate a new surface triangulation with the desired element size distribution. This triangulation is then used as the initial front to generate a volumetric finite element grid of tetrahedral elements using an advancing front technique. Adaptive background grids are used in order to specify curvature-dependent element size distributions that result in volumetric grids with a roughly uniform number of elements in any cross-section of the model.

The region growing approach requires the proper selection of a seed voxel and an intensity range. This has to be done on a trial-and-error basis. However, quite complex vascular trees can be reconstructed using this approach. Another limitation of the method is that for a given intensity threshold intersections between close vessels can be obtained. One of such intersections was generated in the model of the circle of Willis shown in Fig. 5c. This false intersection was then discarded when the model was cut at several locations.

The tubular deformable model is a very reliable semi-automatic method for reconstructing arterial branches independently. Due to its intrinsic smoothing constraints, false intersections with other close vessels are not generated. This approach requires the specification of the arterial axis, which can be done manually or using skeletonization algorithms. Another limitation of this method is that pathological entities that are not tubular in nature, such as aneurysms, will not be properly treated.

The grid generation from surface triangulations has the advantage of avoiding the need of splitting the surface into patches and fitting analytical functions. However, this approach requires several surface processing operations such as merging, smoothing, cutting and optimization. These operators also allow for the possibility of using different segmentation techniques for different entities, such as vessels and aneurysms, which can then be combined into a single model.

The use of adaptive background grids to specify curvature-dependent element size distributions is very useful to reduce the total number of elements in the final grids, while maintaining a reasonable mesh resolution everywhere. Using uniform element size distributions in cases with large variations in spatial scales would result in several millions of elements, and therefore very long computing times.

The methodology has been previously validated using a glass phantom of the carotid artery with stenosis [Cebral at al., 2001]. Errors in the reconstructed radii were less than one percent. We intend to further evaluate this methodology using *in vivo* data from different imaging modalities.

References

Aylward S, Bullit E, Pizer S, Eberly D. Intensity ridge and widths for tubular object segmentation and description. In proceedings of the IEEE Workshop, Mathematical Methods in Biomedical Image Analysis, June 1996.

Berger, SA. Flow in large vessels, in Contemporary Mathematics: Fluid Dynamics in Biology, Cheer AY, van Dam CP, Editors. American Mathematical Society, 1993, 141: 479-518.

Cebral JR, Löhner R. From medical images to CFD meshes. In proceedings of the 8th International Meshing Roundtable, South Lake Tahoe, California, October 10-13, 1999, 321-332.

Cebral JR, Löhner R, Burgess JE. Computer simulation of cerebral artery clipping: relevance to aneurysm neuro-surgery planning. In proceedings of ECCOMAS 2000, John Wiley and Sons, Barcelona, Spain, September 11-14, 2000.

Cebral JR, Löhner R, Choyke PL, Yim PJ. Merging of intersecting triangulations for finite element modeling. *Journal of Biomechanics*, in press 2001.

Cebral JR, Löhner R. From medical images to anatomically accurate finite element grids. *International Journal for Numerical Methods in Engineering*, 51:985-1008, 2001.

Cebral JR, Yim PJ, Löhner R, Soto O, Marcos H, Choyke PL. New methods for computational fluid dynamics modeling of carotid artery from magnetic resonance angiography. In proceedings of SPIE Medical Imaging 2001: Physiology and Function from Multidimensional Images, 2001, 4321: 177-187.

Cebral JR, Löhner R, Soto O, Choyke PL, Yim PJ. Patient-specific simulation of carotid artery stenting using computational fluid dynamics. In proceedings of MICCAI 2001, Utretch, Netherlands, October 2001.

Choyke PL, Yim PJ, Marcos H, Mullick R, Summers R, Ho V. Hepatic MR angiography: a multiobserver comparison of visualization methods. *American Journal of Roentgenology*, 176:465-470, 2001.

Cline HE, Lorensen WE, Souza SP, Jolesz FA, Kikinis R, Gerig G, Kennedy TE. 3D surface rendered MR images of the brain and its vasculature. *Journal of Computer Assisted Tomography*, 15:344-351, 1991.

Frangi AF, Niessen WJ, Hoogeveen RM. Model-based quantitation of 3-D magnetic resonance angiographic images. *IEEE Transactions on Medical Imaging*, 18:946-956, 1999.

Ilegbusi OJ, Hu Z, Nesto R, Waxman S, Cyganski D, Kilian J, Stone PH, Feldman CL. Determination of blood flow and endothelial shear stress in human coronary artery in vivo. *Journal of Invasive Cardiol*ogy, 11(11):667-674, 1999.

Ku DN, Gibbens DP, Zarins CK, Glagov S. Pulsatile flow and atherosclerosis in the human carotid bifurcation: positive correlation between plaque location and low and oscillating shear stress. *Atherosclerosis*, 5:293-302, 1985.

Lei T, Udupa JK, Saha PK, Odhner D. MR Angiographic visualization and artery-vein separation. In proceedings of SPIE Medical Imaging, 1999, 3658:58-66.

Löhner R, Baum JD. Adaptive h-refinement on 3-d unstructured grids for transient problems. *International Journal for Numerical Methods in Fluids*, 14:1407-1419, 1992.

Löhner R. Regridding surface triangulations. *Journal of Computational Physics*, 126:1-10, 1996.

Löhner R. Progress in grid generation via the advancing front technique. *Engineering with Computers*, 12:86-210, 1996.

Löhner R. Automatic unstructured grid generators. *Finite Elements in Analysis and Design*, 25:111-134, 1997.

Milner JS, Moore JA, Rutt BA, Steinman DA. Hemodynamics of human artery bifurcations: computational studies with models reconstructed from magnetic resonance imaging of normal subjects. *Journal of Vascular Surgery*, 27:143-156, 1998.

Moore JA, Steinman DA, Holdsworth DW, Ethier CR. Accuracy of computational hemodynamics in complex arterial geometries reconstructed from magnetic resonance imaging. *Annals of Biomedical Engineering*, 27:32-41, 1999.

Owen SJ. A survey of unstructured mesh generation technology. In proceedings of the 7th International Meshing Roundtable, Sandia National Lab., 1998, 239-267.

Perktold K, Hofer M, Karner G, Trubel W, Schima H. Computer simulation of vascular fluid dynamics and mass transport: optimal design of arterial bypass anastomoses. In proceedings of ECCOMAS 98, John Wiley & Sons, 1998, 2:484-489.

Quarteroni A, Tuveri M, Veneziani A. Computational vascular fluid dynamics: problems, models and methods. *Computing and Visualization in Science*, 2:163-197, 1998.

Steinman DA, Poepping TL, Tambasco M, Rankin RN, Holdsworth DW. Flow patterns at the stenosed carotid bifurcation: effect of concentric versus eccentric stenosis. *Journal of Biomechanics*, 28:415-423, 2000.

Taubin G. A signal processing approach to fair surface design. In proceedings of Computer Graphics, 1995, 351-358.

Taylor CA, Hughes TJR, Zarins CK. Finite element modeling of blood flow in arteries. *Computer Methods in Applied Mechanics and Engineering*, 158:155-196, 1998.

Taylor CA, Draney MT, Ku JP, Parker D, Steele BN, Wang K, Zarins CK. Predictive medicine: computational techniques in therapeutic decision-making. *Computer Assisted Surgery*, 4:231-247, 1999.

Taylor CA, Parker D, Wang KC. Image based geometric modeling of the human aorta. In proceedings of the ASME-BED Bioengineering Conference, vol. 50, 2001, 623-624.

Wentzel JJ, Whelan DM, van Der Giessen WJ, van Beusekom HMM, Andhyiswara I, Serruys PW, Slager CJ and Kram R. Coronary stent implantation changes 3d vessel geometry and 3d shear stress distribution. *Journal of Biomechanics*, 33:1287-1295, 2000.

Wentzel JJ, Krams R, Schuurbiers JC, Oomen JA, Kloet J, van Der Giessen WJ, Serruys PW, Slager CJ. Relationship between neointimal thickness and shear stress after wallstent implantation in human coronary arteries. *Circulation*, 103(13):1740-5, 2001.

Yim PJ, Kim D, Lucas C. High resolution four-dimensional surface reconstruction of the right heart and pulmonary arteries. In proceedings of SPIE Medical Imaging, 1998, 3338:726-738.

Yim PJ, Summers MR. Analytic surface reconstruction by local threshold estimation in the case of simple intensity contrasts. In proceedings of SPIE Medical Imaging, 1999, 3660:288-300.

Yim PJ, Mullick R, Summers RM, Marcos H, Cebral JR, Löhner R, Choyke PL. Measurement of stenosis from magnetic resonance angiography using vessel skeletons. In proceedings of SPIE Medical Imaging, 2000.

Yim PJ, Summers RM, Choyke PL. Gray-scale skeletonization of small vessels in magnetic resonance angiograms. *IEEE Transactions on Medical Imaging*, 19:568-576, 2000.

Yim PJ, Cebral JR, Mullick R, Choyke PL. Vessel surface reconstruction with a tubular deformable model. Submitted to *IEEE Transactions on Medical Imaging*, 2001.

Zarins CK, Giddens DP, Bharadvaj BK, Sottiurai VS, Mabon RF, Glagov S. Carotid bifurcation atherosclerosis. quantitative correlation of plaque localization with flow velocity profiles and wall shear stress. *Circulation Research*, 53(4):502-514, 1983.

Zhao SZ, Xu XY, Hughes AD, Thom SA, Stanton AV, Ariff B, Long Q. Blood flow and vessel mechanics in a physiologically realistic model of a human carotid arterial bifurcation. *Journal of Biomechanics*, 33: 975-984, 2000.